LA-UR -82-793

CONF-820334--2

TITLE: LASER-SHOCK-WAVE SIMULATION OF TWO-DIMENSIONAL NUCLEAR SHOCK WAVES

AUTHOR(S): M. D. Wilke, S.N. Stone, G.E. Barasch

SUBMITTED TO: Defense Nuclear Agency Conference on Instrumentation for Nuclear Weapons Effects

University of California

LOS ALAMOS SCIENTIFIC LABORATORY
Post Office Box 1663 Los Alamos, New Mexico 87545

Form No. 836 R1
St. No. 2629

LASER SHOCK WAVE SIMULATION OF TWO-DIMENSIONAL NUCLEAR SHOCK WAVES

M.D. Wilke, S.N. Stone, G.E. Barasch

(Los Alamos National Laboratory)

We will describe results from experiments that used shock waves generated by a high-power laser to simulate multi-dimensional nuclear shocks. The shocks were produced in 50 torr air by irradiating hollow plastic shell targets with 30J, 300 ps Nd-glass laser pulses. We first investigated the individual near-spherical shocks to determine over what range the shock radius, R_s, obeyed the Taylor-von-Neumann-Sedov expansion law, $R_s \alpha t^{2/5}$. The relationship was found to hold for 0.9 cm $\leq R_s \leq$ 2.0 cm. We also modeled the shocks with the nuclear effects code RADFLO and found good agreement between calculation and data for R_s vs t and also gas and electron densities determined from two-wavelength interferograms of the shock waves. Based on our understanding of the individual shocks we next designed two experiments to investigate two-dimensional shock waves. The first experiment consisted of reflecting a spherical shock off a plastic block suspended 0.9 cm above the target. In the second experiment, two identical spherical shocks were simultaneously generated 1.9 cm apart and allowed to collide. The reflected shocks were compared through scaling laws to the Teapot/Met shock wave generated from a 22KT nuclear explosion 1224 above the ground. The mach structures were found to be similar. We then modeled the reflecting and interacting shocks with a two-dimensional effects code using the one-dimensional RADFLO output to start the problem. Calculation and data for Mach angles and triple point propagation were found to be in good agreement.

INTRODUCTION

Studies of the interactions of strong planar shock waves with their own reflections or a second shock wave have been conducted for some time using shock tubes. The only existing data for strong spherical shock wave interactions are from nuclear shocks reflected from ground planes. By strong spherical shock waves we mean those where the spherical shock wave radius, R_s, obeys the Taylor-Von Neumann-Sedov[1] relation $R_s \alpha t^{2/5}$ where t is the time from shock initiation. Studies of spherical shock wave interactions have been conducted using high explosives,[2] however the comparatively low ratio of the yield to the source-mass and the large volume over which the energy is released, severely limit the time during which the $R_s \alpha t^{2/5}$ relation holds.

It has been known for some time[3] that focused laser breakdown of gasses at near-atmospheric pressures or irradiation of targets in low pressure gases will produce strong near-spherical shock waves. By including the energy dependence in the Taylor-von Neumann-Sedov relation and comparing it with radii versus time measurements, it is also possible to estimate the laser-target coupling efficiency.[4,5]

In the experiments described here we used laser generated shock waves to simulate spherical nuclear shock wave interactions for comparison to a scaled nuclear event and for comparison to nuclear effects computer code calculations.

EXPERIMENTAL PROCEDURE

Figure 1 is a schematic of a double shock wave experiment and the diagnostic layout. The details are described elsewhere.[6] A two-beam Nd:glass laser was used to irradiate the targets with up to 40J per beam in 300 ps pulses. The 8.6 cm beams were focused to 100 μM spots with ∿ f/4 aspheric lenses. The 3.4 μg hollow plastic shell targets were 500 μM in diameter with 4 μM thick walls and were supported by 10 μM glass stalks.

The diagnostics included a two-wavelength holographic ruby-laser interferometer, a shadowgraphy camera, an emission framing camera, a gated microchannel plate image-intensifying ($MCPI^2$) camera, and a vacuum bi-planar photodiode. The ruby laser included a doubling crystal to produce light at 347.2 nm as well as 694.3 nm. The interferometer was operated in the two wavelength mode without the shadowgraphy system or in the single 694.3 nm wavelength mode with the shadowgraphy system by inserting the blue reflecting red transmitting mirrors M1 and M2. One 20 ns interferogram was exposed per shot, per wavelength. The fringe shift-vs-position information from the interferograms was Abel inverted to obtain index of refraction-vs-radius data. The sets of data from interferograms made at two wavelengths were used to unfold electron and gas density profiles. The details of the unfolding have been reported elsewhere.[7]

The electrostatic emission framing camera produced ten, 10 ns exposures 50 ns apart and the $MCPI^2$ camera gave a single 4 ns exposure with good

spatial resolution but large timing jitter. The shadowgraphy camera was framed at 1 frame-per- s and gave 200 ns exposures. The emission cameras were useful from $0 \leq t \leq 1$ s when the shocks were luminous. The shadowgraphy and interferometer systems were used during 400 ns$\leq t \leq$30 μs.

The majority of the experiments were conducted with the target chamber air pressure at 50 torr and a few experiments were conducted with 1 torr chamber pressure. There was a small amount of laser induced air breakdown next to the targets in the 50 torr experiments. The air breakdown and asymmetric target illumination led to initially aspherical shock waves as shown in the MCPI[2] photograph in Fig. 2. The 50 torr shocks became spherical by 1 μs. Because of the asymmetry, the 50 torr shock centers were displaced ~0.15 cm toward the Nd:laser beam from the target position. There was no apparent laser induced air breakdown at 1 torr and therefore the 1 torr shocks were initially very spherical and remained centered on the target. The 50 torr data were preferred in these experiments because 50 torr shocks produced better shadowgrams and interferograms throughout the shock wave development.

The radii from the emission photographs were obtained by taking one-half the largest distance across the emitting region perpendicular to the Nd:laser beam (see Fig. 2). Therefore the lobed regions in Fig. 2 were ignored. Radii from the shadowgraphs and interferograms were measured from the shock center.

The interferogram radii could be measured with the most accuracy. However, only one interferogram was obtained at each wavelength per shot. We therefore took interferograms of several shots at a constant delay time while varying the Nd:glass laser energy, E_L, from shot to shot over the range 5J$\leq E_L \leq$10J. We found that we could very accurately fit the measured

shock radii, R_s, versus E_L by using $E_L = aR_s^b$. Once the a and b were determined for a given delay time, we could interpolate an R_s for a chosen E_L. We also applied this technique to the $MCPI^2$ data, however, $MCPI^2$ trigger jitter resulted in poor fits to the measured E_L-vs-R_s points.

RESULTS

ONE DIMENSIONAL (1-d) EXPERIMENTS

We first examined the properties of individual shock waves to determine over what range $R_s \alpha t^{2/5}$ and to determine how well we could numerically calculate the other measured shock properties (i.e. electron and gas densities, and optical power versus time). Figure 3 is a plot of R_s-vs-t where the R_s were interpolated from the 50 torr E_L-vs-R_s data assuming E_L=25J. Over 0.6 cm $\leq R_s \leq$ 2 cm (0.7 $\mu s \leq t \leq$ 10 μs) the data accurately follow the $R_s \alpha t^{2/5}$ curve. After 10 μs the shock begins to slow to sonic velocity and before 0.7 μs the influence of target mass and irradiation asymmetry, discussed elsewhere[7] is apparent.

The 1-d Lagrangian nuclear fireball computer code RADFLO[8] was used to calculate the shock wave properties. Figure 4 is a comparison of interpolated interferometric R_s-vs-t data from Fig. 3 with computed R_s-vs-t. Also plotted are the emission framing camera R_s-vs-t from E_L=25J, 1 torr and 50 torr experiments, and a single interferometer point at 1 torr. The computer calculations assumed an initial shock wave energy E_s, of 12.3J and 2.5J for the shocks in 1 torr and 50 torr air respectively. Therefore, laser-target coupling is $\sim$50% at 1-torr and $\sim$10% at 50 torr. Laser-target coupling is less at 50 torr because of the air breakdown (see Ref. 7). "Cent." implies that the calculation was started by depositing all the energy in the hollow center of the target and "Unif." implies the calculation was started by depositing the energy in the target mass M_t so that $\epsilon = E_s/M_t$ was constant throughout the part of the computational mesh representing the target.

Figure 5 compares calculated peak gas density versus time with the measured peak gas density from the interferometry data for shocks in 50 torr air. Figure 5 also compares the electron density measured at the center of the shock versus time with calculations. In both cases, agreement is good.

Figure 6 is a comparison of peak-normalized calculated and measured optical power versus time. The calculations in Fig. 5 and 6 were performed with the Centaur energy input. There is a small difference between the measured and calculated times of peak optical power but there is good agreement in general between the curve shapes. The decrease in the optical power of the 1 torr shock at ~100 ns is caused by disassembly of the target plasma. The power output increases again as the expanding target material shocks the surrounding air. In 50 torr air, the target material shocks the air quickly and there is no decrease in emission before shock formation.

TWO DIMENSIONAL (2-d) EXPERIMENTS

Based on the 1-d individual shock experimental results we chose a separation of 1.8 cm between the two targets for double shock wave experiments. The 2-d experiments were conducted in 50 torr air. Because of the ~0.15 cm displacement of the shock centers from the targets in 50 torr air, the shock centers were actually ~2.1 cm apart. Reflecting shock wave experiments were conducted using a clear acrylic block as a reflecting plane suspended above the target at a distance of 0.9 cm. The block passed the 694.3 nm interferometry light. A slight shift in the fringes within the block was detected which was caused by density waves in

the block. The density waves were generated by the air shock colliding with the block surface. The fringe shift was sufficiently small to conclude that the block behaved like an ideal refelcting surface.

An interferogram of a reflecting shock is shown in the second part of Fig. 7 and a set of shadowgraphs of two 50 torr colliding shocks is shown in Fig. 9. As a shock collides with a reflecting plane or an identical shock and a critical angle of intersection is reached, the Mach stem forms (see Fig. 8). The height of the intersection of the Mach shock wave and the original shock (known as the triple point) gradually increases as the shock expands.

We first compared the reflected laser shock wave in the second part of Fig. 7 to the scaled nuclear shock wave generated by Teapot/Met shown in the first part of Fig. 7. The scaling laws used to compare the two shocks are[9]

$$\frac{D'}{D} = \frac{t'}{t} = \left(\frac{E_s'}{E_s}\ \frac{P_o}{P_o'}\right)^{1/3} . \qquad (1)$$

We have used D to indicate the distance from the reflecting plane to the shock center, P_o is the ambient pressure and, as before, E_s is the shock wave energy. Table I is a comparison between parameters describing Teapot/Met and parameters describing the laser shock. The laser shock E_s was determined by fits to HADFLO and the Taylor-von Neumann-Sedov law. Note the factor of 4×10^{13} between the E_s values.

If we take the Teapot/Met values as the primes in Eq. 1 then the quantity on the right is 1.4×10^{4}. $D'/D=1.4\times10^{4}$ and $t'/t=1.1\times10^{4}$. A better comparison would have been possible if the interferogram was exposed at t=12 μs.

The shocks in Fig. 7 were compared by superimposing the shock wave centers and reflecting planes with a photographic enlarger and tracing the shock boundaries. The schematic is given in Fig. 8. It appears as though the nuclear Mach stem is riding up on the precursor which is a result of fireball heating of the ground. Considering the $4x10^{13}$ magnitude difference in the E_s ratio, the shocks compare very well.

We next attempted to model the laser shocks with a version of the 2-d hydrodynamics code YAQUI[10] that has previously been used to model nuclear shock wave interactions.[11] The YAQUI calculation was begun by picking up the previously described "Cent " RADFLO calculation when the shock radius reached 0.8 cm. The results are shown in Fig. 10. The data in Fig. 10 is described in Table II. Note that the calculated Mach stem forms at about the same time as the laser shock Mach stem forms in the shadowgraphy sequence of Fig. 9. Agreement between calculated and measured shock boundaries is very good.

CONCLUSION

The laser shock waves can be used to simulate nuclear shock interactions when properly scaled. The laser shock properties are readily calculable using nuclear effects computer codes. Diagnosing the laser shock simulations is much easier than high explosive shock simulations because there are no destructive forces. In general, the laser shock wave simulation technique provides a useful tool for studying strong spherical shock interactions . More exotic simulations such as preheat of the reflecting plane to simulate fireball-ground preheat for investigations of effects such as precursor formation may also be possible.

The technique is limited. Combinations of high laser power and ambient pressure lead to more severe air breakdown. The air breakdown limits the achievable source energy densities.

TABLE I: COMPARISON OF FIG. 7 SHOCK WAVES

	Teapot/Met	Laser Shock
E_s	22KT (9.2×10^{13}J)	2.5J
D	1.22×10^4 cm	0.9 cm
P_o	700 torr	50 torr
t	170 ms	15 s

TABLE II: TWO-DIMENSIONAL SHOCK INFORMATION FOR FIG. 10

No.	Time (s)	Energy (J)	Description
1	10.0	16.8	Shock and reflecting plane
2	10.5	28.8	B-shock of double-shock expri-ment E_L C-beam) = 30.7 J
3	15.0	20.1	Shock and reflecting plane
4	15.0	22.4	Shock and reflecting plane
5	20.0	26.0	B-shock of double-shock experi-ment E_L(C-beam) = 22.4 J
6	20.0	22.1	Shock and reflecting plane
7	20.0	28.3	Shock and reflecting plane
8	30.0	24.8	Shock and reflecting plane

TABLE II: TWO-DIMENSIONAL SHOCK INFORMATION FOR FIG. 10

No.	Time (μs)	Energy (J)	Description
1	10.0	16.8	Shock and reflecting plane
2	10.5	28.8	B-shock of double-shock expri-ment E_L(C-beam) = 30.7 J
3	15.0	20.1	Shock and reflecting plane
4	15.0	22.4	Shock and reflecting plane
5	20.0	26.0	B-shock of double-shock experi-ment E_L(C-beam) = 22.4 J
6	20.0	22.1	Shock and reflecting plane
7	20.0	28.3	Shock and reflecting plane
8	30.0	24.8	Shock and reflecting plane

REFERENCES

1. Taylor, G., "The Formation of a Blast Wave by a Very Intense Explosion: I. Theoretical Discussion, "Proc. Roy. Soc. 201 (1950), p. 159.

2. Dewey, J.M. McMillin, D.J., and Classen, D.F., "Photogrammetry of Spherical Schocks Reflected from Real and Ideal Surfaces," J. Fluid Mech., 81 (1977), p. 701.

3. Hughes, T.P., Plasmas and Laser Light, John Wiley and Sons, New York (1975).

4. Basov, N.G., Gamaly, E.G., Krokhin, O.N., Mikhailov, Yu. A., Sklizkov, G.V., and Fedotov, S.I., "Investigation of Plasma Parameters at the Spherical Heating of the Isolated Solid Target by High-Power Laser Radiation," in Laser Interaction and Related Plasma Phenomena (edited by Schwarz and Hora), Vol. 3b, New York, Plenum Press (1973), p. 553.

5. Leonard, T.A., and Mayer, F.J., "Helium Blast-Wave Measurements of Laser-Heated Microballoon Targets," J. Appl. Phys. 46 (1975), p. 3562.

6. Wilke, M.D., and Stone, S.N., "Optical Diagnostic System for Observation of Laser Produced Shock Waves," SPIE Vol. 191 (LASL Optics Conference) (1979).

7. Wilke, M.D. Thesis, U. of Colo. at Boulder, "Laser Shock Wave Generation, Propagation and Interactions in Low Pressure Air," (1981), Los Alamos Report LA-9184-T.

8. Zinn, J., "A Finite Difference Scheme for Time-Dependent Spherical Radiation Hydrodynamics Problems," J. Comp. Phys. 14 (1974), p. 569.

9. Glasstone, S., "The Effects of Nuclear Weapons, U.S. Atomic Energy Commission (1962).

10. Hirt, C.W., Amsden, A.A., and Cook, J.L., "An Arbitrary Lagrangian-Eulerian Computing Method for all Flow Speeds," J. Comp. Phys. 14 (1974), p. 227.

11. Sandford, M.T. II, Anderson, R.C., Horak, H.G., and Kodis, J.W., "Improved, Implicit Radiation Hydrodynamics," J. Comp. Phys. 19 (1975), p. 280.

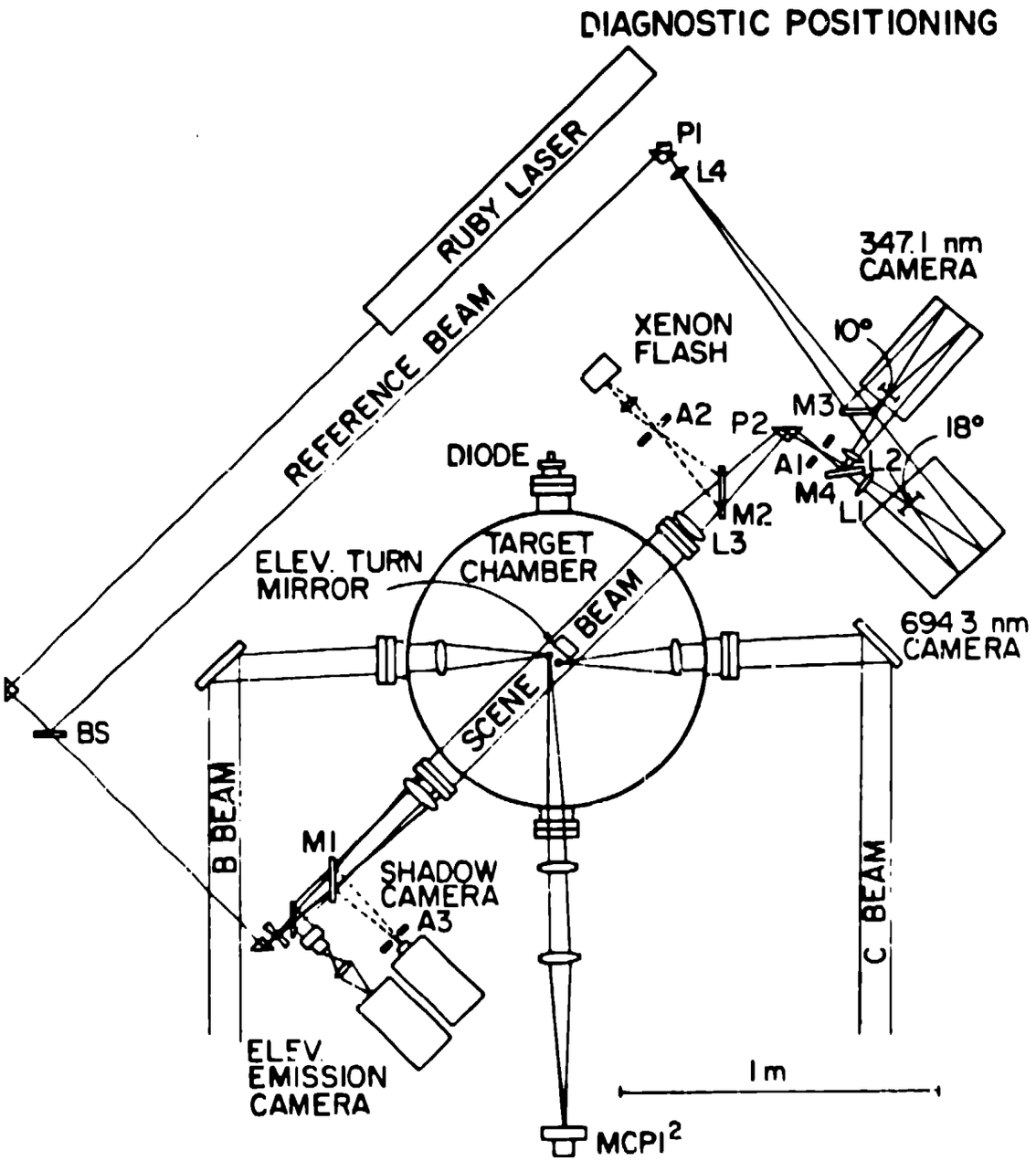

Fig. 1. Schematic layout of diagnostics and beam alignment for a double-shock experiment.

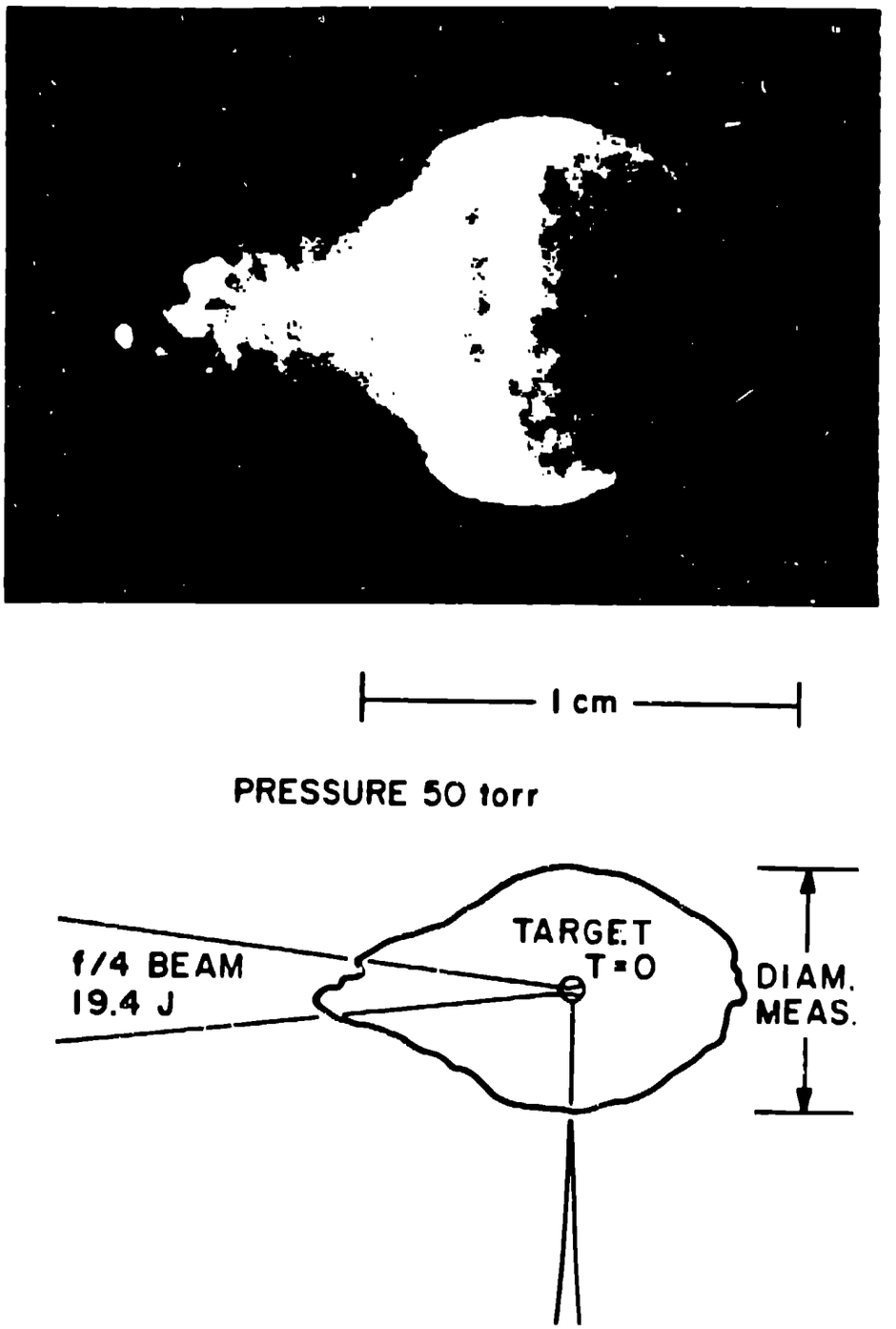

Fig. 3. Microchannel plate image-intensifier picture. Exposure was at ~ 200 ns with large error due to trigger jitter.

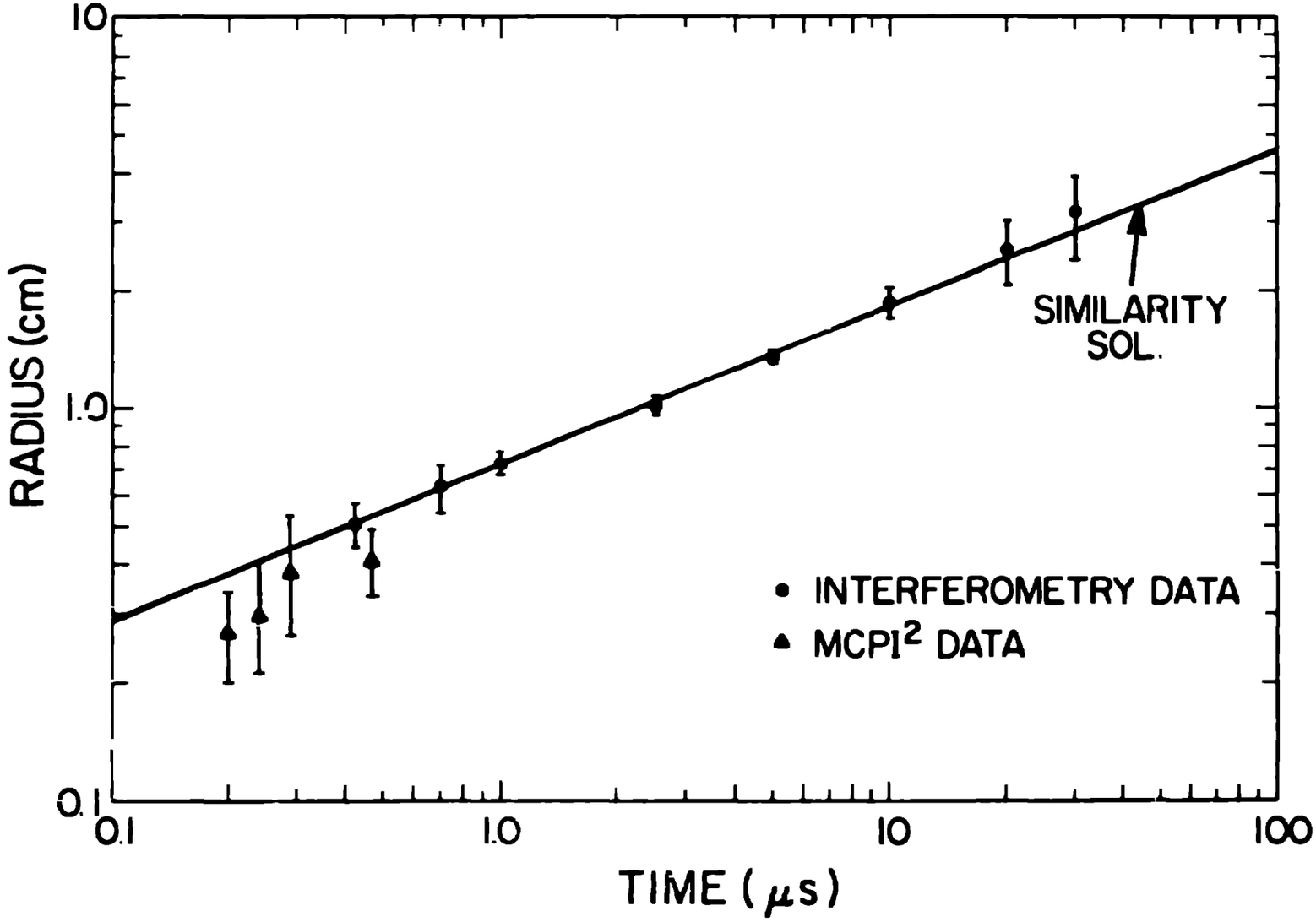

Fig. 3. Radius-vs-time points interpolated from radius-vs-E_L MCPI^2 and interferometry data. Similarity Sol. is $R_s \propto t^{2/5}$

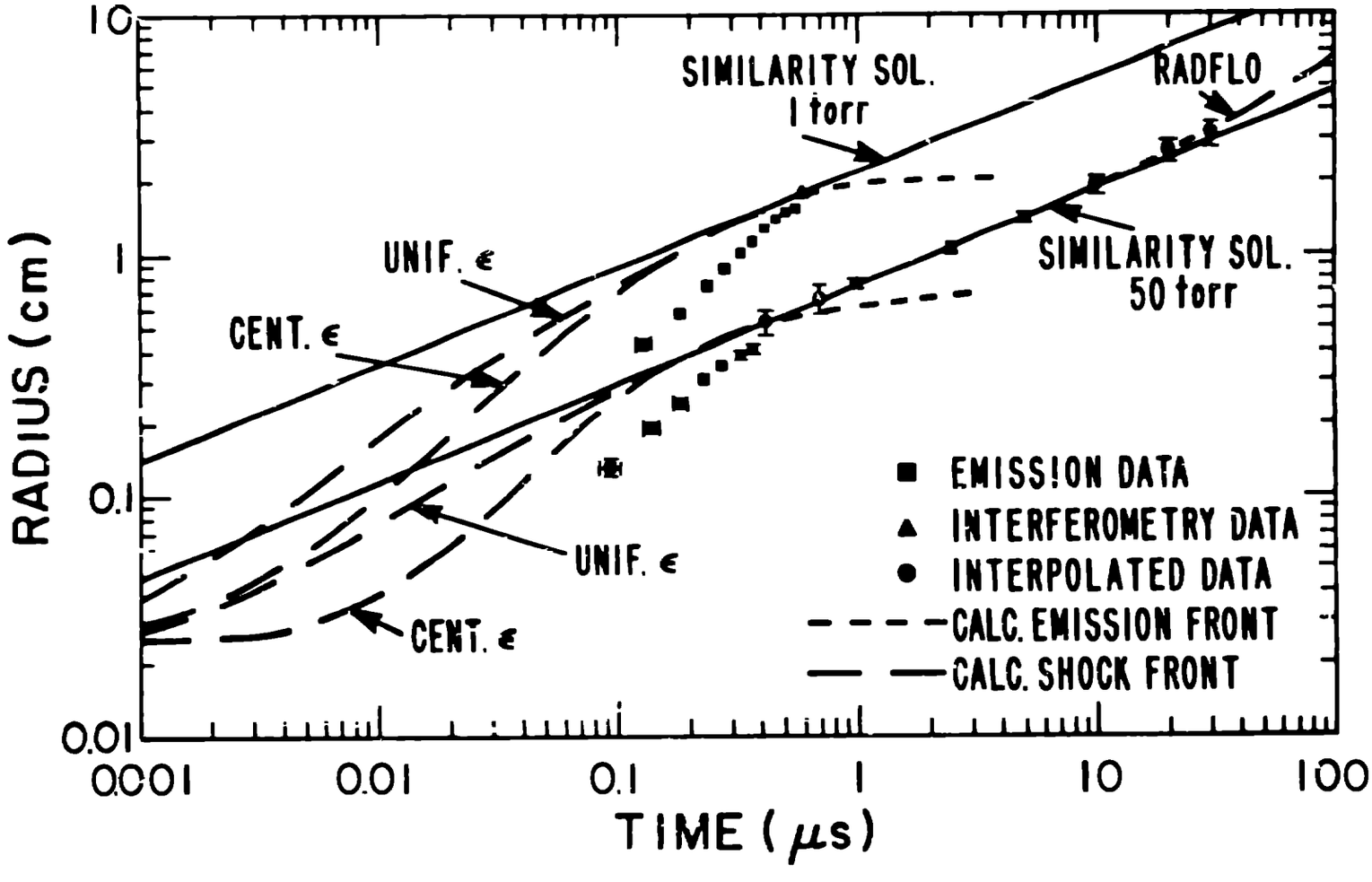

Fig. 4. Comparison of numerically calculated and measured radii-vs-time for shocks in 1-torr and 50-torr air. UNIF. ε and CENT. ε calculations are described in text.

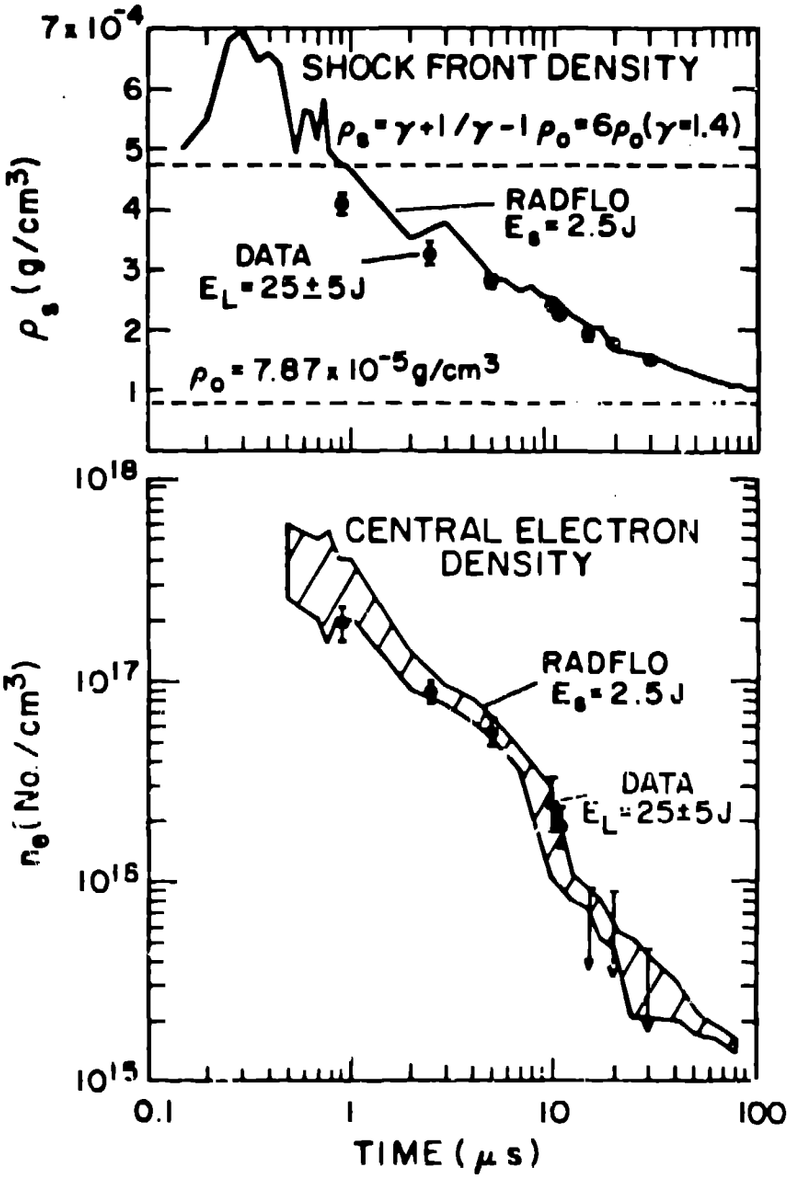

Fig. 5. Comparison of theoretically calculated and measured peak gas densities and central electron densities versus time.

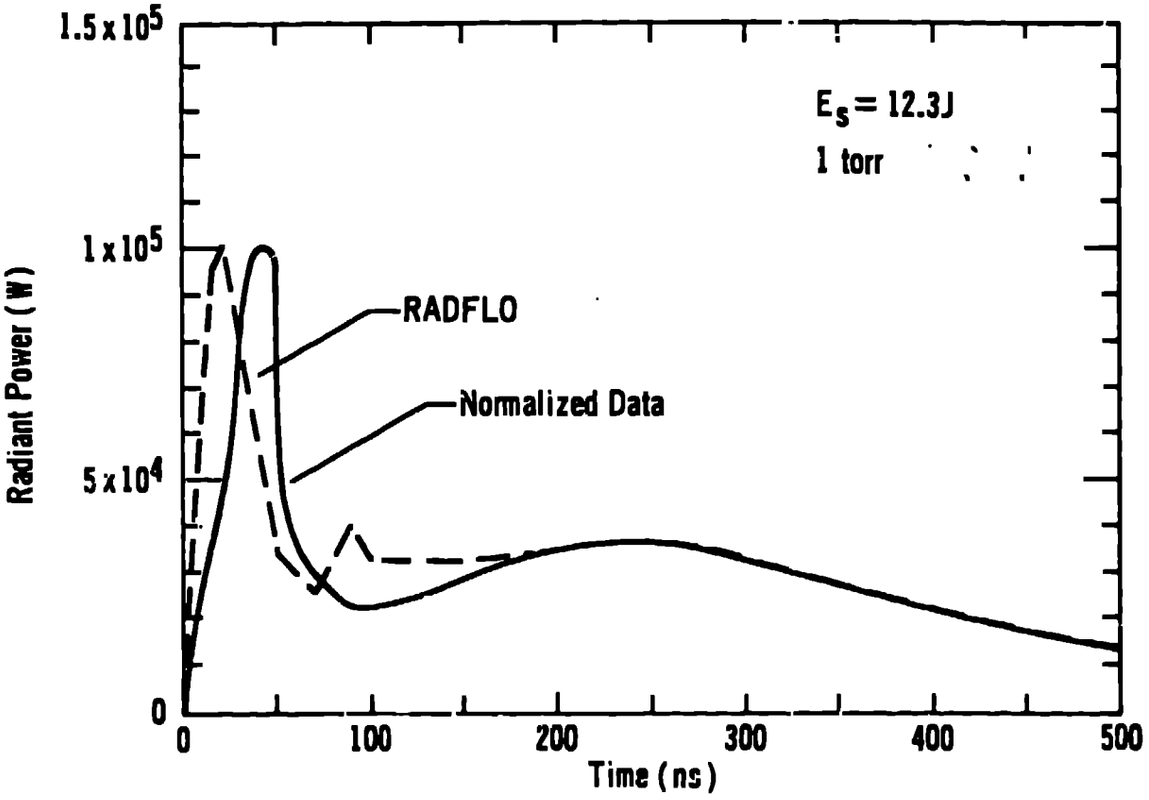
1.5x10^5
1x10^5
5x10^4
0
Radiant Power (W)
E_s = 12.3J
1 torr
RADFLO
Normalized Data
0
100
200
300
400
500
Time (ns)

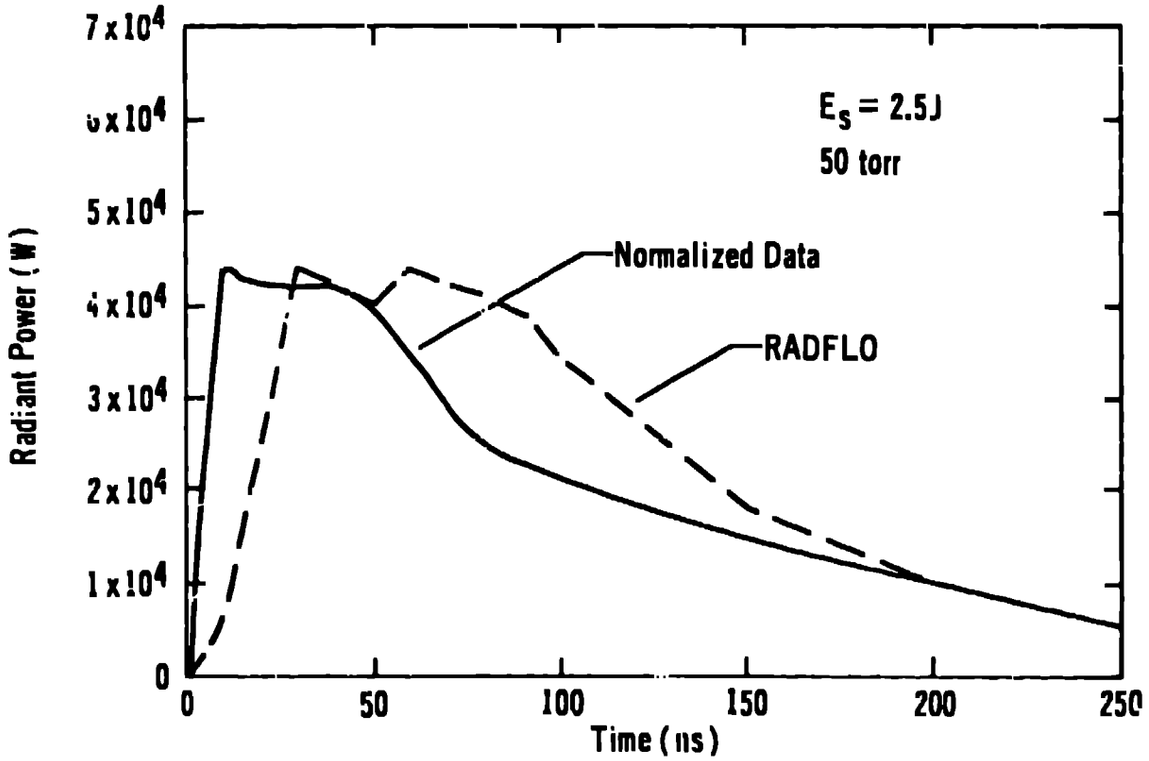
7x10^4
6x10^4
5x10^4
4x10^4
3x10^4
2x10^4
1x10^4
0
Radiant Power (W)
E_s = 2.5J
50 torr
Normalized Data
RADFLO
0
50
100
150
200
250
Time (ns)

Teapot/Met event (22 kt, 122 m above the ground) at t = 170 ms.

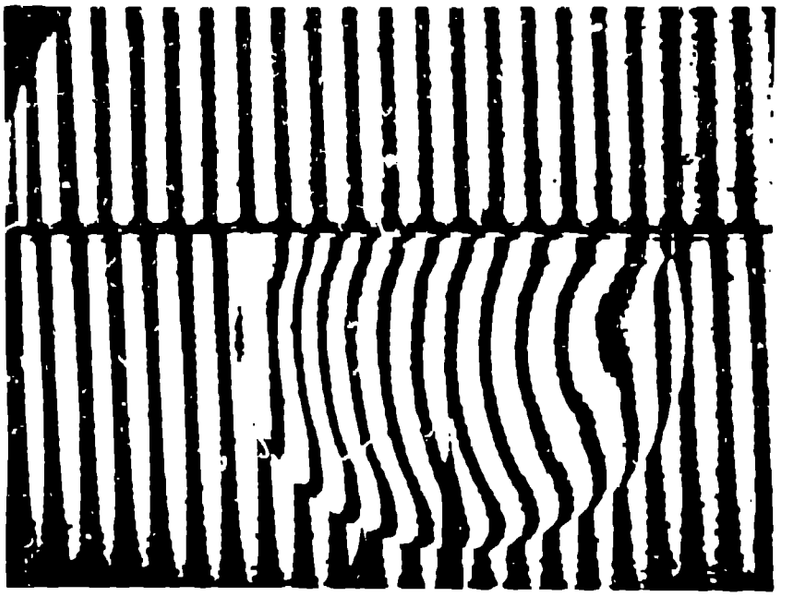

50-torr, E_L = 20.1 J laser shock wave at t = 15 ns.

Fig. 7. Comparison of a large-scale, low-altitude nuclear shock with a reflected laser shock

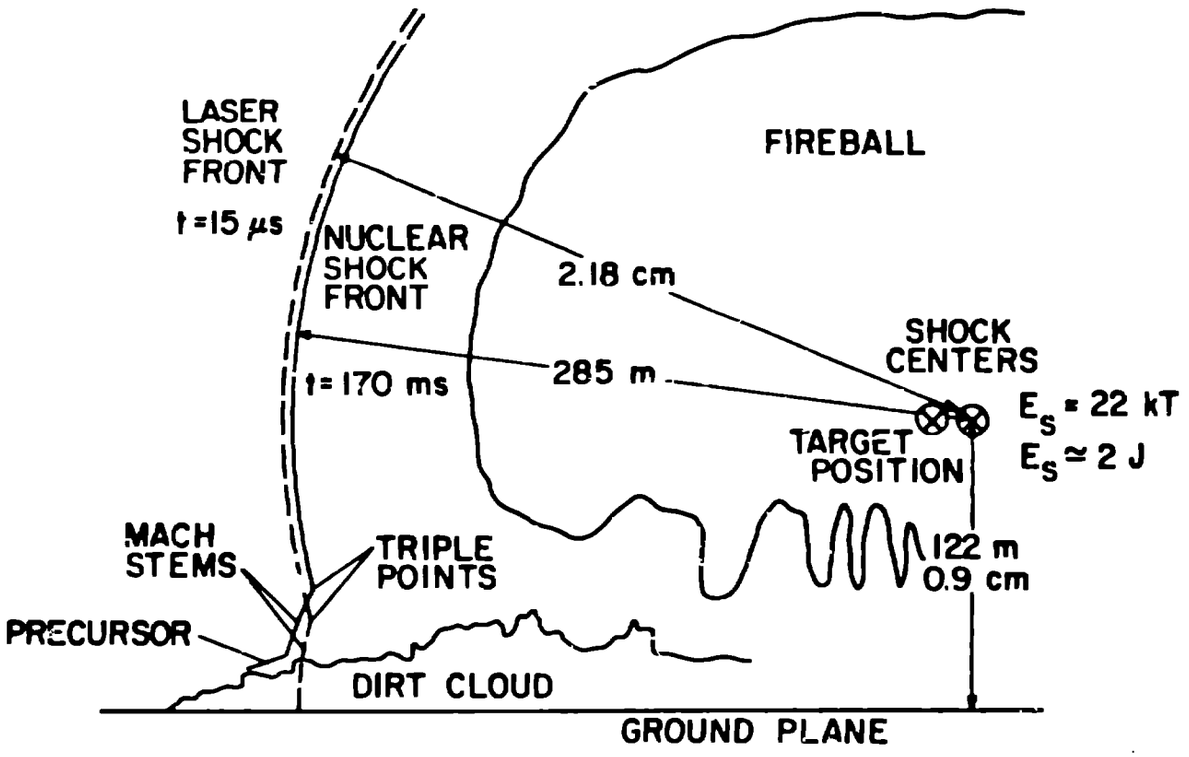

Fig. 8. Schematic comparison of left side of the laser shock in Fig. 7 with the Teapot/Met shock. Comparison was made by superimposing shock centers and reflecting planes, and then tracing shock boundaries.

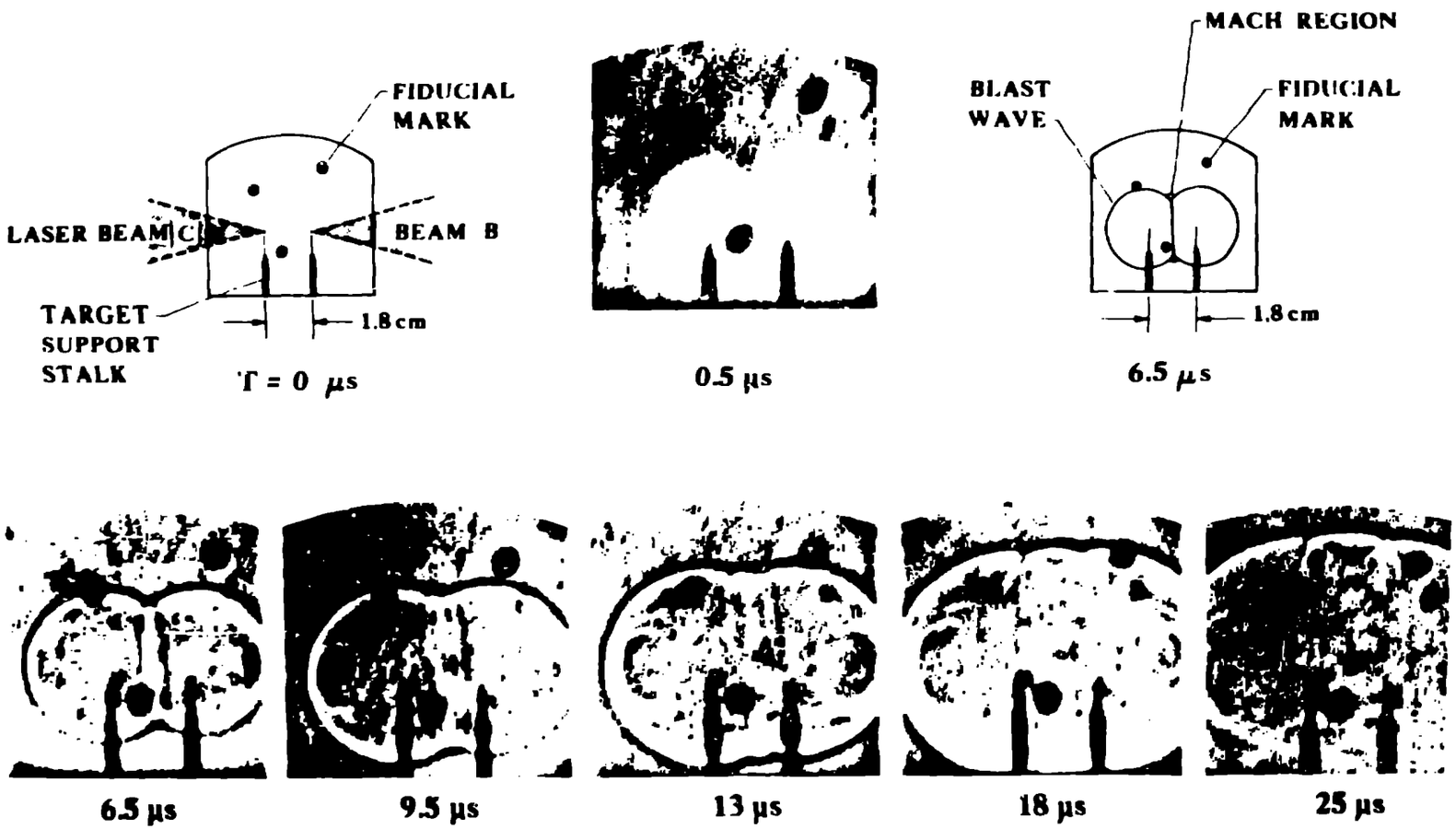

Fig. 9. Composite of shadowgraphy sequences of 50 torr double shocks, with E_L = 25 J for each shock.

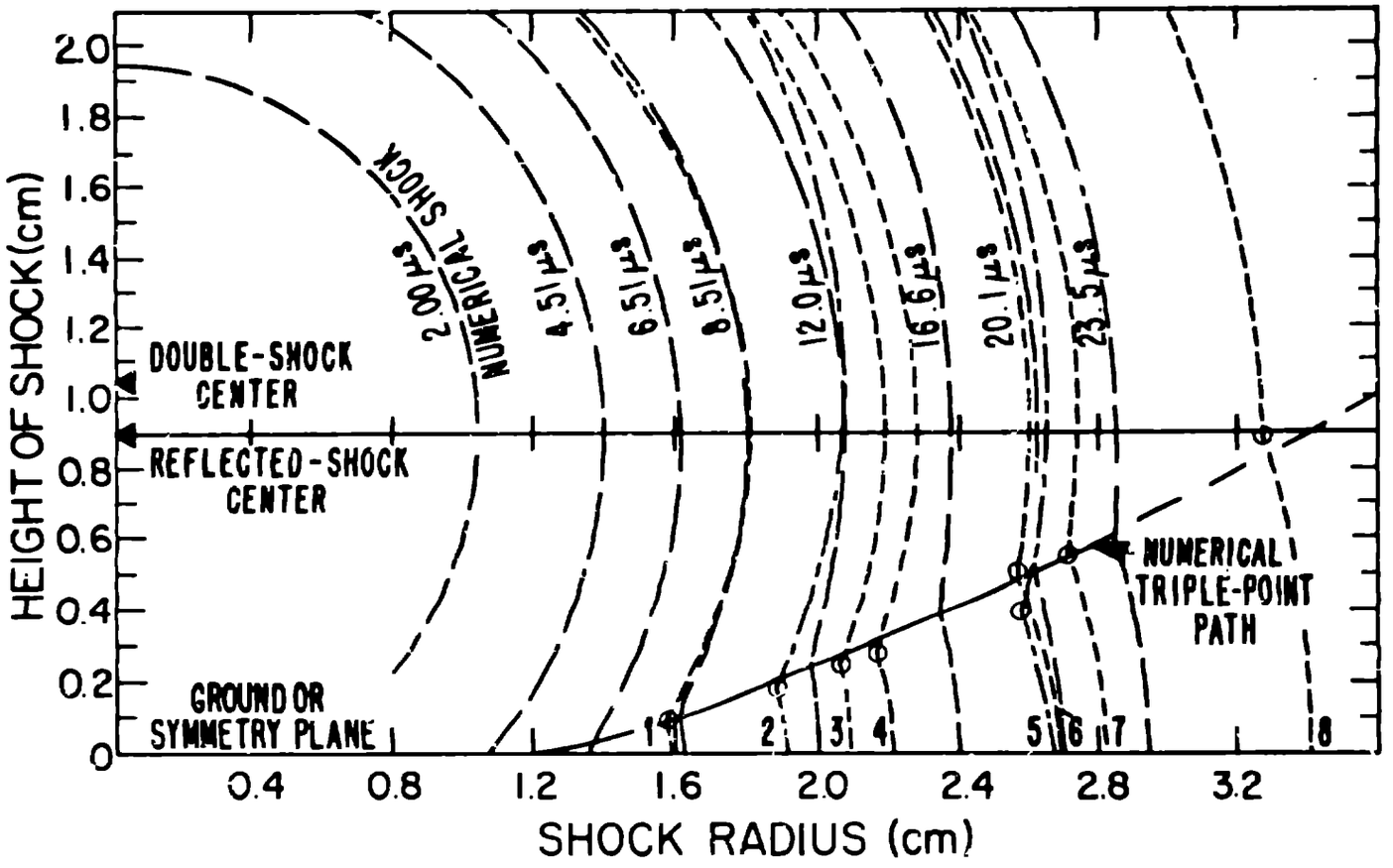

Fig. 10. Comparison of numerically calculated shock boundaries (long dashes) with experimental shock boundaries (short dashes and long-short dashes). See Table II for descriptions.